Effect of Stacking Interactions on Charge Transfer States in Photoswitches Interacting with Ion Channels

Vito F. Palmisano, Shirin Faraji, Juan J. Nogueira

Table of Contents

1 Initial Structures

Detailed information regarding the initial structures of both $Na_V1.4$ human's brain ion channel (PDB ID: 6AGF) and the ligands can be found in a previous article [1].

2 Molecular Dynamics Simulations

In a previous study [1], classical molecular dynamics (MD) and Gaussian Accelerated MD simulations were performed to map the phase space of the central pore of the $Na_v1.4$ ion channel. Then, the binding free energy was computed by the 1-Average-Molecular Mechanics Generalized Born Surface Area method to identify the most stable binding pockets for azobenzene (AZ) and p-diaminoazobenzene (pAZ). From the most stable binding pocket, the final snapshot of the simulation was selected for evolving further MD simulations in the present study. These additional MD simulations were performed for AZ and pAZ integrated in the $Na_v1.4$ ion channel, and in water and hexane. The simulations were performed with the CUDA [2] version of the Amber20 package [3].
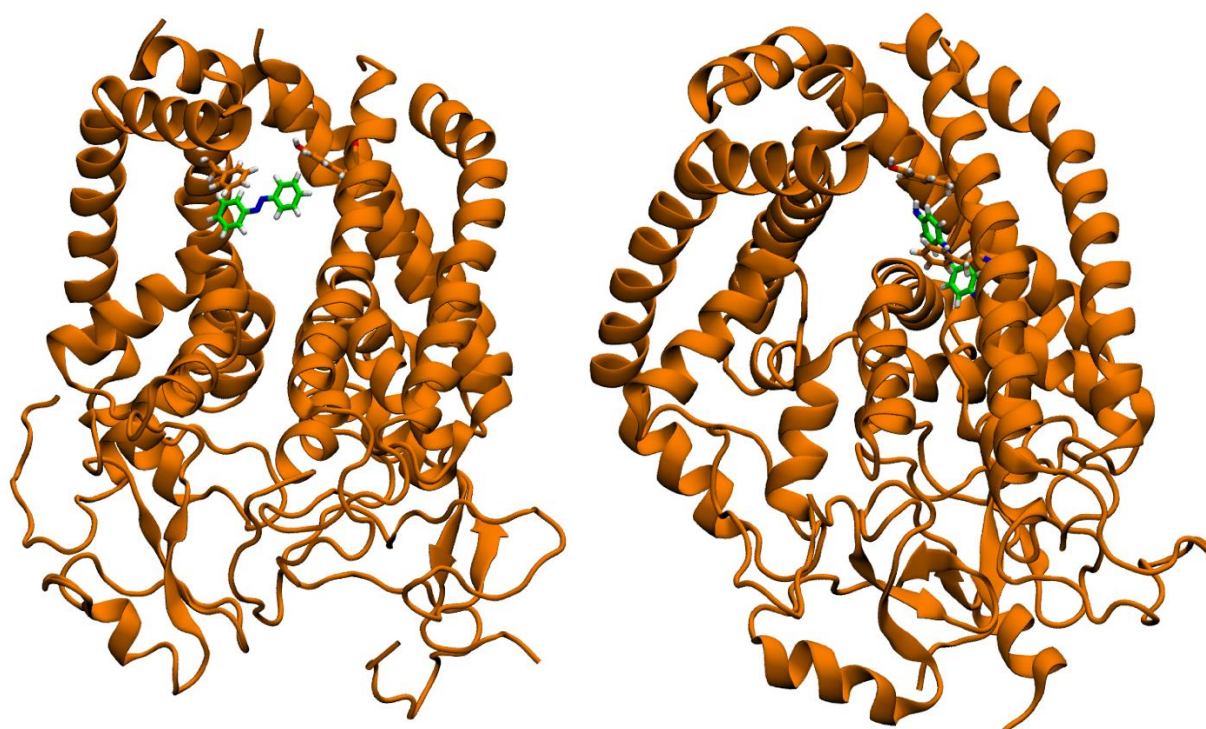
Figure 1: Representation of AZ (left) and pAZ (right) interacting with the $Na_v1.4$ channel. The snapshots were taken from the MD simulation of the unmutated channel.

2.1 Computational Details for AZ and pAZ Interacting with $Na_V1.4$

The two photoswitch/channel systems contained 98497 atoms for AZ/$Na_v1.4$ and 98499 for pAZ/$Na_v1.4$. First, an energy minimization was carried out with the steepest descent method for 5000 steps, followed by additional 5000 steps using the conjugate gradient method. Then, NVT heating and NPT equilibration simulations were carried out with positional restraints for amino acid residues and for the membrane lipids. The restraint force constants used along the dynamic protocol are listed in Table 1. A NVT heating at 303.15K over 120 ps was performed, using the Langevin thermostat (friction coefficient 1.0 ps) to control the temperature. Then, the desired density was achieved by running an equilibration in the NPT ensemble with a Monte Carlo barostat and a semi-isotropic pressure scaling in three steps of 100 ps each, sequentially decreasing the restraints on the protein and lipids, and an unrestrained step of 4000 ps. Finally, an unconstrained production run was carried out at 303.15 K and 1.0 bar for 100 ns for both AZ and pAZ systems. During the full protocol, electrostatic interactions were calculated by means of the particle-mesh Ewald method with a grid spacing of 1.0 Å; hydrogen bond lengths were kept fixed using the SHAKE algorithm; the van der Waals cutoff radius and switching distance were set to 12.0 and 10.0 Å, respectively; the time step was set to 2 fs. The same exact procedure was performed for the P797Y mutated $Na_v1.4$ ion channel interacting with AZ.

Table 1: Value of the force constant of the restraint potential used during the MD simulations.

| Run | Force Constants | |
	Protein Restraints	Lipid Restraints
1 (NVT)	10	10
2 (NPT)	5	5
3 (NPT)	2.5	2.5
4 (NPT)	1	1
5 (NPT)	0	0

2.2 Computational Details for AZ and pAZ in Water

The systems formed by AZ and pAZ in water contain 5636 and 5638 atoms, respectively. First, an energy minimization was carried out with the steepest descent method for 5000 steps, followed by additional 5000 steps using the conjugate gradient method. An NVT heating at 303.15 K over 100 ps was performed with the Langevin thermostat (friction coefficient 1.0 ps). Then, the desired density was achieved by running an equilibration in the NPT ensemble with a Monte Carlo barostat and isotropic pressure scaling in one step of 1000 ps. Finally, an unconstrained production run was carried out at 303.15 K and 1.0 bar for 100 ns for both AZ and pAZ systems. During the full protocol, the van der Waals cutoff radius and switching distance were set to 12.0 and 10.0 Å, respectively; electrostatic interactions were calculated by means of the particle-mesh Ewald method with a grid spacing of 1.0 Å; hydrogen bond lengths were kept fixed using the SHAKE algorithm; and a time step of 2 fs was used.

2.3 Computational Details for AZ and pAZ in Hexane

The systems formed by AZ and pAZ in hexane contain 4046 and 4048 atoms, respectively. First, an energy minimization was carried out with the steepest descent method for 5000 steps, followed by conjugate gradient method for 5000 steps. An NVT heating at 303.15 K over 100ps was performed with the Langevin thermostat (friction coefficient 1.0 ps). Then, the desired density was achieved by running an equilibration in the NPT ensemble with a Monte Carlo barostat and isotropic pressure scaling in one step of 1000 ps. Finally, an unconstrained production run was carried out at 303.15 K and 1.0 bar for 100 ns for both AZ and pAZ systems. During the full protocol, the van der Waals cutoff radius and switching distance were set to 12.0 and 10.0 Å, respectively; electrostatic interactions were calculated by means of the particle-mesh Ewald method with a grid spacing of 1.0 Å; hydrogen bond lengths were kept fixed using the SHAKE algorithm; and a time step of 2 fs was used.

3 QM/MM vertical excitation energies

3.1 Vertical Excitations

From the 100 ns MD simulations of AZ and pAZ interacting with Na$_v$1.4, water and hexane, 100 equidistant snapshots were extracted from the last 90 ns of each simulation for computing the excitation energy by QM/MM calculations. The MoBioTools package was used to extract the geometries, split the system in the QM and MM region and prepare the input for the QM/MM calculations [4]. The system was split into two regions, the AZ and pAZ in the QM region and the environment (Na$_v$1.4 system, water and hexane) in the MM region. The electrostatic QM/MM scheme implemented in Gaussian 09 was employed, with 10 roots to compute the vertical excitation energies at TD-DFT level by using the ωB97XD functional and cc-pVDZ basis set [5,6,7]. To obtain the absorption spectra of the photoswitches, the QM/MM excitation energies for the 100 geometries were convoluted with Gaussian functions with full width at half-maximum of 0.30 eV and heights proportional to the oscillator strengths of the electronically excited states. Then, the most intense band is scaled to unity, and the other bands are scaled by the same factor. The density of states for each transition type was computed in the same way but the Gaussian heights are equal to unity and not proportional to the oscillator strengths. The identification and characterization of electronic states was performed by inspecting the natural orbitals involved in the excitations as well as examining numerical descriptors defined in the TheoDORE package, such as the charge transfer (CT) number [8]. In particular, to distinguish between the nπ* and $\pi\pi$* excitations, the AZ and pAZ molecules were split into two fragments, one containing the central nitrogen atoms and another one containing the rest of the molecule. An electronic state with the position of hole (POS$_i$ in Table 2) lower than 1.4 is considered as a nπ* state, while it is considered to be $\pi\pi$* otherwise. This descriptor was chosen since

the central nitrogen atoms correspond to fragment 1 where the n orbital is mainly localized. Table 2 below shows the output of the TheoDORE analysis for a representative snapshot of the MD simulation, with AZ included in the QM region for the excited state calculations.

Table 2: Electronic properties predicted by the TheoDORE analysis for the ten lowest excited singlet states. "dE" is the excitation energy in eV, "f" is the oscillator strength, "POS" is the average position between fragment 1 and fragment 2 of the electron, "POSi" is the position of the hole created after excitation, "POSf" is the position of the excited electron, and "CT" is the charge transfer number.

State	dE(eV)	f	POS	POSi	POSf	CT
S_1	2.460	0.000	1.267	1.216	1.317	0.390
S_2	4.278	0.642	1.657	1.864	1.450	0.532
S_3	4.729	0.015	1.815	1.972	1.658	0.369
S_4	4.975	0.027	1.844	1.940	1.749	0.306
S_5	5.383	0.023	1.688	1.895	1.481	0.528
S_6	5.525	0.068	1.622	1.326	1.918	0.667
S_7	5.649	0.032	1.655	1.411	1.899	0.677
S_8	5.808	0.065	1.697	1.613	1.780	0.601
S_9	6.082	0.048	1.798	1.795	1.802	0.369
S_{10}	6.231	0.037	1.815	1.746	1.885	0.327

Table 3 below represents the two fragments in which the molecules were arbitrarily divided (the azo group and the rest of the molecule) with the relative electron/hole density. For the $S_1(n\pi^*)$ state, the hole population is mainly located in the azo group (0.79), while the excited electron is more delocalized along the molecules, with 0.69 population in the azo group and 0.31 in the rest of the molecules. In the case of the $S_2(\pi\pi^*)$, the hole is more localized in the benzene rings (0.86) and the excited electron is again delocalized among the benzene rings (0.45) and the azo group (0.45). Similar information can be extracted from the natural transition orbitals involved in the main transitions of these two electronic states (Figure 2a).

Table 3: Hole electron population analysis of the $S_1(n\pi^*)$ and $S_2(\pi\pi^*)$ states.

		S_1		
Fragment	h+	e-	sum	diff
Azo	0.79055	0.68886	1.47940	0.10169
Rings	0.21793	0.31962	0.53755	-0.10169
Total	1.00848	1.00848	2.01696	-0.00000

		S_2		
Fragment	h+	e-	sum	diff
Azo	0.13653	0.55300	0.68953	-0.41647
Rings	0.86946	0.45299	1.32245	0.41647
Total	1.00599	1.00599	2.01198	-0.00000
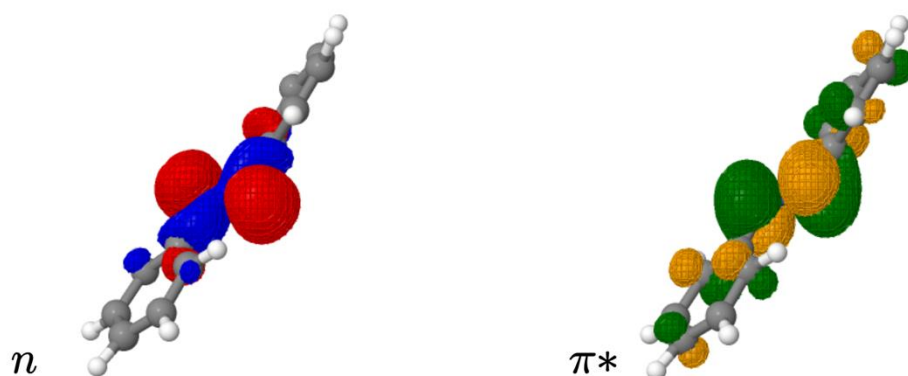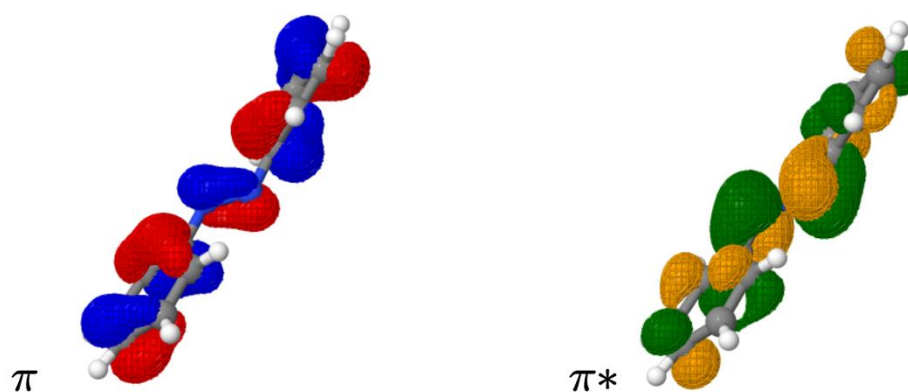
Figure 2: Natural Transition Orbitals involved in the main transitions of the $S_1(n\pi^*)$ and $S_2(\pi\pi^*)$ states for AZ (QM region) interacting with the protein.

3.2 Charge Transfer Characterization

From the 100 ns MD simulation AZ and pAZ in complex with the $Na_v1.4$ and P797Y mutated $Na_v1.4$ channels, 100 equidistant snapshots were extracted from the last 90 ns of each simulation for QM/MM calculations. As explained above, the MoBioTools package was used to extract the geometries, split the system in the QM and MM regions and prepare the input for the QM/MM calculations. The closest residues to the ligands AZ and pAZ along the dynamics were obtained by a contact analysis performed with CPPTRAJ[9]. Then, the closest aromatic residues were included in the QM region with AZ and pAZ. Specifically, five different sets of excited-state QM/MM calculations were performed. These calculations differ in the residues included in the QM region: AZ-P797, AZ-Y1593, pAZ-1586, pAZ-Y1593 and the mutated AZ-P797Y. For each set, 100 QM/MM calculations were performed. The MoBioTools software was also employed to complete the valence of the QM by the link atom approach. The electrostatic QM/MM scheme implemented in Gaussian 09 was employed. 10 roots were computed at TD-DFT level with ωB97XD functional and cc-pVDZ basis set. The identification and characterization of electronic states was performed by inspecting the natural orbitals involved in the excitations and by transition density analysis using the TheoDORE package. In particular, $n\pi^*$ and $\pi\pi^*$ states were identified as explained in the previous section. In addition, the intermolecular CT state, characterized by electron transfer from the protein residues to the chromophore, was identified by computing the CT number between two fragments defined by the ligand (AZ or pAZ) and the aminoacid included in the QM region. Table 4 below shows the results of the TheoDORE analysis for a representative snapshot of the MD simulation, with AZ-P797Y included in the QM region for the excited state calculations.

Table 4: Electronic properties predicted by the TheoDORE analysis for the ten lowest excited singlet states for the system for which the QM region is formed by AZ-P797Y. "dE" is the excitation energy in eV, "f" is the oscillator strength, "POS" is the average position between fragment 1 and fragment 2 of the electron, "POSi" is the position of the hole created after excitation, "POSf" is the position of the excited electron, and "CT" is the charge transfer number.

state	dE(eV)	f	POS	POSi	POSf	CT
S_1	2.164	0.000	1.998	1.997	1.998	0.004
S_2	4.077	0.647	1.994	1.994	1.994	0.004
S_3	4.249	0.001	1.504	1.014	1.994	0.981
S_4	4.434	0.014	1.993	1.989	1.997	0.013
S_5	4.726	0.015	1.997	1.995	1.998	0.006
S_6	4.851	0.054	1.010	1.008	1.013	0.014
S_7	5.220	0.024	1.960	1.923	1.996	0.080
S_8	5.514	0.007	1.923	1.868	1.979	0.146
S_9	5.604	0.030	1.520	1.222	1.818	0.604
$S1_0$	5.633	0.078	1.152	1.087	1.218	0.144

The first two excitations show a full localization of the electrons in fragment 2 (the AZ molecule), since they are local excitation in AZ, while the third transition goes from the tyrosine to AZ (CT state).

Table 5: Hole electron population analysis of the $S_1(n\pi^*)$, $S_2(\pi\pi^*)$ and $S_3(CT)$ states.

S_1				
Fragment	h+	e-	sum	diff
Tyr	0.00289	0.00154	0.00442	0.00135
AZ	1.00630	1.00765	2.01394	-0.00135
Total	1.00918	1.00918	2.01836	-0.00000

S_2				
Fragment	h+	e-	sum	diff
Tyr	0.00577	0.00647	0.01224	-0.00071
AZ	1.00191	1.00120	2.00311	0.00071
Total	1.00767	1.00767	2.01535	0.00000

S_3				
Fragment	h+	e-	sum	diff
Tyr	0.98642	0.00577	0.99219	0.98064
AZ	0.01352	0.99416	1.00768	-0.98064
Total	0.99993	0.99993	1.99987	0.00000

(a)

n $\pi*$

(b)

π $\pi*$

(c)

CT $\pi*$
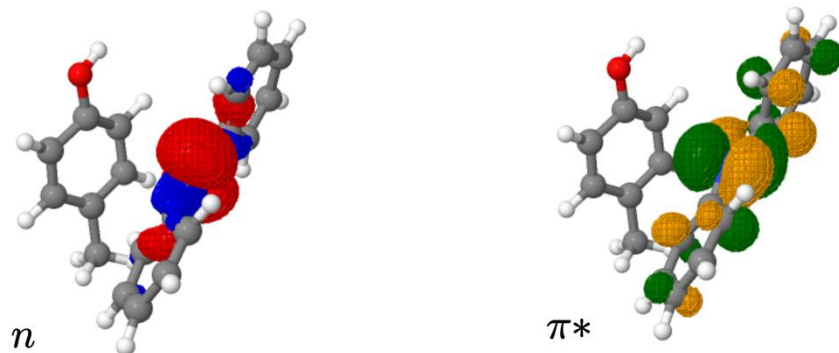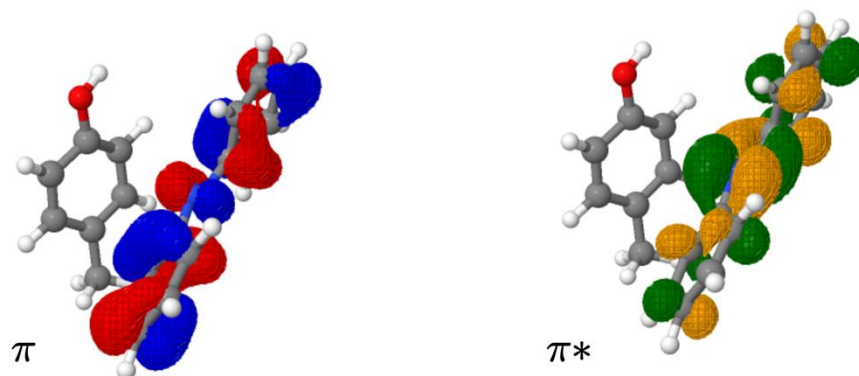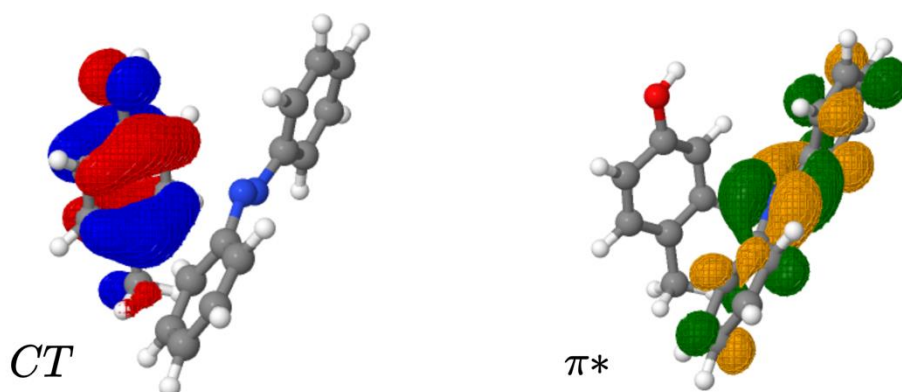
Figure 3: Natural Transition Orbitals involved in the main transitions of the $S_1(n\pi*)$, $S_2(\pi\pi*)$ and $S_3(CT)$ states for AZ-F797Y in the QM region.

4 Vacuum Calculations

The calculations in vacuum for AZ and pAZ were performed using Gaussian 09 software. The calculations included AZ and pAZ isolated in vacuum and interacting in a parallel and t-shaped conformations with phenylalanine (P) and tyrosine (Y) (truncated at the alpha carbon), which are the residues observed to interact

with the chromophores along the Na$_v$1.4/AZ-pAZ MD simulations. Figure 4 shows the parallel, t1-shaped and t2-shaped conformations for the AZ-phenylalanine case.

parallel conformation   t1-shaped conformation   t2-shaped conformation
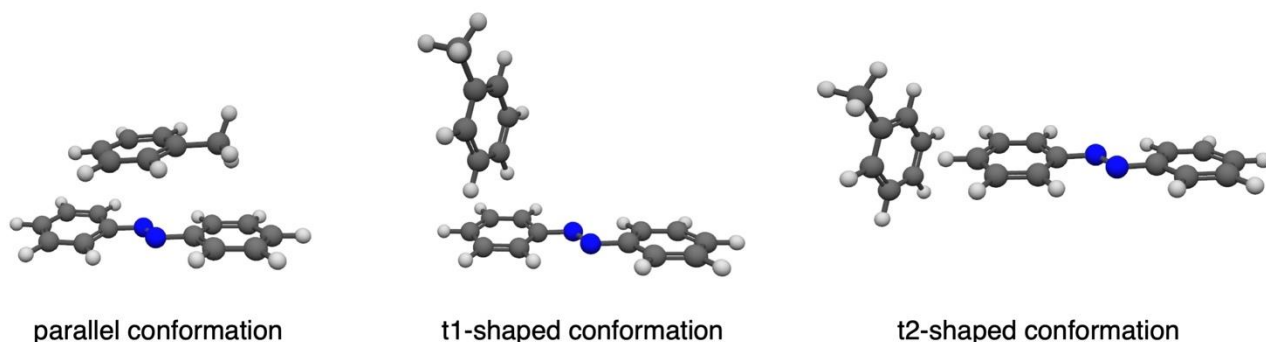
Figure 4: Face-to-face, t1-shaped and t2-shaped conformations for the AZ-phenylalanine case considered in the calculations.

The calculations were performed at TD-DFT level with ωB97XD functional and cc-pVDZ basis set. The identification of the local nπ* and ππ* states and intermolecular CT states was achieved as explained above.

References

[1] Palmisano, V. F.; Gómez-Rodellar, C.; Pollak, H.; Cárdenas, G.; Corry, B.; Faraji, S.; Nogueira, J. J. Binding of azobenzene and p-diaminoazobenzene to the human voltage-gated sodium channel Nav1.4. *Physical Chemistry Chemical Physics* **2021,** *23* (5), 3552.

[2] Salomon-Ferrer, R.; Gotz, A. W.; Poole, D.; Le Grand, S.; Walker, R. C. Routine microsecond molecular dynamics simulations with AMBER on GPUs. 2. Explicit solvent particle mesh Ewald. *Journal of chemical theory and computation* **2013,** *9* (9), 3878.

[3] D.A. Case, K. Belfon, I.Y. Ben-Shalom, S.R. Brozell, D.S. Cerutti, T.E. Cheatham, III, V.W.D. Cruzeiro, T.A. Darden, R.E. Duke, G. Giambasu, M.K. Gilson, H. Gohlke, A.W. Goetz,R Harris, S. Izadi, S.A. Izmailov, K. Kasavajhala, A. Kovalenko, R. Krasny, T. Kurtzman, T.S. Lee, S. LeGrand, P. Li, C. Lin, J. Liu, T. Luchko, R. Luo, V. Man, K.M. Merz, Y. Miao, O. Mikhailovskii, G. Monard, H. Nguyen, A. Onufriev, F. Pan, S. Pantano, R. Qi, D.R. Roe, A. Roitberg, C. Sagui, S. Schott-Verdugo, J. Shen, C.L. Simmerling, N.R. Skrynnikov, J. Smith, J. Swails, R.C. Walker, J. Wang, L. Wilson, R.M. Wolf, X. Wu, Y. Xiong, Y. Xue, D.M. York and P.A. Kollman **2020**, AMBER 2020, University of California, San Francisco.

[4] G. Cárdenas, J. Lucia-Tamudo, H. Mateo-delaFuente, V. F. Palmisano, N. Anguita-Ortiz, L. Ruano, Á. Pérez-Barcia, S. Díaz-Tendero, M. Mandado and J. J. Nogueira, MoBioTools: A Toolkit to Setup QM/MM Calculations, *ChemRxiv*, **2022**

[5] Frisch, M. J.; Trucks, G. W.; Schlegel, H. B.; Scuseria, G. E.; Robb, M. A.; Cheeseman, J. R.; Scalmani, G.; Barone, V.; Mennucci, B.; Petersson, G. A.; Nakatsuji, H.; Caricato, M.; Li, X.; Hratchian, H. P.; Izmaylov, A. F.; Bloino, J.; Zheng, G.; Sonnenberg, J. L.; Hada, M.; Ehara, M.; Toyota, K.; Fukuda, R.; Hasegawa, J.; Ishida, M.; Nakajima, T.; Honda, Y.; Kitao, O.; Nakai, H.; Vreven, T.; Montgomery, J. A., Jr.; Peralta, J. E.; Ogliaro, F.; Bearpark, M.; Heyd, J. J.; Brothers, E.; Kudin, K. N.; Staroverov, V. N.; Kobayashi, R.; Normand, J.; Raghavachari, K.; Rendell, A.; Burant, J. C.; Iyengar, S. S.; Tomasi, J.; Cossi, M.; Rega, N.; Millam, J. M.; Klene, M.; Knox, J. E.; Cross, J. B.; Bakken, V.; Adamo, C.; Jaramillo, J.; Gomperts, R.; Stratmann, R. E.; Yazyev, O.; Austin, A. J.; Cammi, R.; Pomelli, C.; Ochterski, J. W.; Martin, R. L.; Morokuma, K.; Zakrzewski, V. G.; Voth, G. A.; Salvador, P.; Dannenberg, J. J.; Dapprich, S.; Daniels, A. D.; Farkas, Ö.; Foresman, J. B.; Ortiz, J. V.; Cioslowski, J.; Fox, D. J. Gaussian 09, Revision E.01, **2009**, Gaussian, Inc., Wallingford CT.

[6] Dunning, Jr., T. H. Gaussian Basis Sets for Use in Correlated Molecular Calculations. I. The Atoms Boron through Neon and Hydrogen *The journal of chemical physics* **1989**, *90*, 1007-1023.

[7] Chai, J.-D.; Head-Gordon, M. Long-range corrected hybrid density functionals with damped atom–atom dispersion corrections. *Physical Chemistry Chemical Physics* **2008,** *10* (44), 6615.

[8] Plasser, F. TheoDORE: A toolbox for a detailed and automated analysis of electronic excited state computations. *The Journal of chemical physics* **2020,** *152* (8), 084108.

[9] Roe, D. R.; Cheatham III, T. E. PTRAJ and CPPTRAJ: software for processing and analysis of molecular dynamics trajectory data. *Journal of chemical theory and computation* **2013,** *9* (7), 3084.w